IEEE Journal of Microwaves

Received 15 September 2020; revised 22 October 2020; accepted 26 October 2020.
Date of current version 7 January 2021.

Digital Object Identifier 10.1109/JMW.2020.3034661

RF Systems Design for Simultaneous Wireless Information and Power Transfer (SWIPT) in Automation and Transportation

DIEGO MASOTTI [1] (Senior Member, IEEE), MAZEN SHANAWANI [1], GHULAM MURTAZA [1], GIACOMO PAOLINI [1] (Graduate Student Member, IEEE), AND ALESSANDRA COSTANZO [2] (Senior Member, IEEE)

(Invited Paper)

[1]Department of Electrical, Electronic and Information Engineering "G. Marconi," University of Bologna, 40136 Bologna, Italy
[2]Department of Electrical, Electronic and Information Engineering "G. Marconi," University of Bologna, 47521 Cesena, Italy

CORRESPONDING AUTHOR: ALESSANDRA COSTANZO (e-mail: alessandra.costanzo@unibo.it).

ABSTRACT This work presents some recent solutions that exploit the wireless power transfer (WPT) technology for energizing moving vehicles and machinery tools. Such technology is currently experiencing unprecedented interests in non-traditional RF/microwave sectors fields, such the industrial automation and the railway transportation safety. Near-field electromagnetic coupling solutions are presented showing that, in order to obtain efficient performances for broad ranges of operating conditions, the nonlinear electromagnetic co-design of the entire WPT system, from the energy source to the receiver load, needs to be carried out. This technology can be combined with wireless data transfer, thus realizing integrated systems able to simultaneously control the energy transfer and the transmission of data. The adopted operating frequencies are in the MHz range, which is only recently considered for this kind of applications. In particular this work focuses on three different systems: the first one demonstrates the constant powering of "on the move" industrial charts at 6.78 MHz, regardless of the relative position of the transmitter and the receiver sub-systems; the second one presents a novel design of a balise transportation system adopting a high efficiency GaN-based transmitter designed to keep its performance over a wide range of loading conditions; the last one consists of the simultaneous wireless power and data transfer, to a rotating machinery tool, automatically controlled by the powering system based on the coexistence of frequency-diverse inductive and capacitive couplings.

INDEX TERMS WPT, inductive coupling, capacitive coupling, nonlinear design, electromagnetic simulation, multi-domain simulation.

I. INTRODUCTION

With the ongoing industrial evolution, in the informatic, communication, and alternative energy sectors, many experts agree that the 4th industrial revolution will bring forward more fusion between the physical and informatic realms [1]. It will be quite important to prepare for a systematic integration between power and communication -or information- systems for many industrial and transportation applications. As for the global demand on oil resources, around 30% is attributed to the transportation sector alone [2], and a similar estimated figure is attributed to various industries. On the other hand, there is increasing deployment of virtual reality [3] in production lines, autopiloting systems in many vehicular [4], and regional trains transportation systems [5]. This brings forward the concept of Simultaneous Wireless Information and Power Transfer (SWIPT) systems, which has been around in the wireless and cellular networks domain for a while [6]–[8]. As it will be demonstrated, the systems have structural differences although they hold the same abbreviation. To the best of our knowledge, this is the first time an article attempts to overview the recent design trends of SWIPT systems used in the transportation and industrial domains.

This work is licensed under a Creative Commons Attribution-NonCommercial-NoDerivatives 4.0 License. For more information, see https://creativecommons.org/licenses/by-nc-nd/4.0/

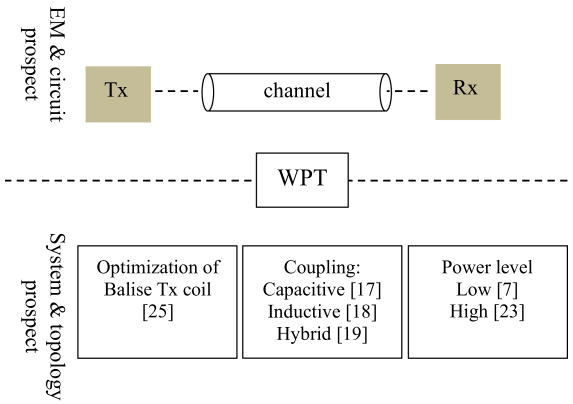

FIGURE 1. Categorization of WPT may be regarded based on either a circuital approach or topological approach.

The paper is organized as follows: the introduction gives a brief presentation of the development of the WPT concept followed by an overview of the different technologies that pertain to the same WPT family.

Then, more insight into the experiments that, to our knowledge, hold good potentiality for future applications are demonstrated. The integration of WPT and communication systems into a SWIPT system will be visited with special focus on the emerging issues.

To make WPT system more apt for modern industrial and transportation applications, the evolvement from a position-dependent system to a position-independent system will be demonstrated in the second section. The integration of the previous WPT system with other communication systems, resulting in a real high-power SWIPT system, is presented in the third section. The fourth section presents simultaneous WPT and communication systems that work in a complementary way to feed sensors and collect their readings wirelessly. The conclusion section will recap the important outcome of the explained cases in order to give the design measures recommended for future designs.

A. DEVELOPMENT OF WPT CONCEPT

The earliest WPT experiments may be traced back to Tesla's experiments for wireless power transmission [9]. Due to reduced efficiency for long distances and the accompanying health and burn hazard of transmitting high-power electromagnetic (EM) signals [10], this research has been idle for several decades until a new suggestion is given by Kurs *et al.* [11] earlier in this century. Their suggestion depends on magnetic resonance where this approach has solved the health concerns connected to high amplitudes of the electric field $\boldsymbol{E}$ [12]. Today, the research trend is to attain at different designs to optimize the power transfer efficiency.

B. WPT EXAMPLES

Fig. 1 shows possible approaches to analyze the WPT system. It can either can be considered as a combination of linear and nonlinear circuit components, where the EM and nonlinear components formulate the entire system. Or it could be approached from a more systematic point of view, that involves the power level, and the available integrated systems.

From the EM & circuit perspective the system is divided into the following subsections:

1) THE TRANSMITTING PART TX

This part includes the oscillation-generating circuitry in addition to the amplification circuit before the transmitting element. The aim here is always to minimize circuit losses before the wireless transmission part. In this context, transmitter circuits based on Class-E, F, EF amplifiers have been designed and tried for constant [13] and variable load [14] cases. Such systems can achieve considerably high efficiency reaching 90% [15]. Most of these systems are based on linear components. Another approach, which is claimed to achieve very high efficiency over a wide range of load circuit impedance is the use of Duffing resonators [16] and nonlinear capacitors which also claim high efficiency around 85%.

2) THE CHANNEL

Is the medium in which the electromagnetic signal propagates. The distance between Tx and Rx varies based on the application which, in turn, identifies whether the EM problem is far-field or near-field. The EM problem is defined as a far-field problem when the distance between Tx and Rx is equal to several wavelengths λ of the RF signal propagating in free space. Empirically, this distance varies between 5 to 10 times of λ. On the other hand, near-field problems usually have less than λ spacing between Tx and Rx.

A few chosen near- and far-field examples from the literature will be demonstrated in the next section. As for the near-field problems, the coupling regime could be capacitive [17], inductive [18], or hybrid [19].

3) THE RECEIVING PART RX

For this part, the general concept is to use half wave, or full wave rectifiers [20]. However, recent advances have been achieved by using synchronous rectification [21].

The overall system performance is controlled by the efficiency of each of the preceding parts. Therefore, the optimization of the linear part -the EM problem- and the nonlinear part -including both transmitting and receiving circuits- will lead to an optimized performance of the entire system.

On the other hand, from the systematic point of view, many noticeable contributions [22]–[24] have been reported. In [25] the authors analyze the performance of a compound communication and WPT system working at $f_c = 4.234$ MHz, and $f_p = 27.095$ MHz, respectively. The analysis is held assuming a moving on-board device at $v = 300$ km/h, to measure the resulting current in the balise. The analysis assumes an electronically small antenna which gives rise to an equal current phase distribution along the transmitting loop antenna. A similar approach is adopted by Zhu, *et al.* [24] with more focus on analyzing the mutual coupling between the different transmitting antennas.

In [23] a more constrained framework is presented for a Wireless Low floor Tram (WTRAM) using a co-simulation approach with the aim to minimize the mass of the WPT system.

In [26] Song *et al.* attempt to analyze the balise behavior using a different approach that involves neural networks. The significance of this approach comes from the possibility to quickly analyze the system without having to run a full electromagnetic simulation each time.

II. WPT FAR-FIELD AND NEAR-FIELD SOLUTIONS

A. FAR FIELD WPT

Many long-haul wireless power transmission systems have been thought of in the past [27] where they have been mostly approached as fixed stations without integrating a communication system. In the recent literature, however, some interesting SWIPT-like examples can be found. The authors in [8] show the operating principle of far-field SWIPT relying on the channel estimation capability, acting as a reverse communication link from the receiver to the transmitter. A preliminary experimental analysis is given in [28] at 2.45 GHz, in a virtual scenario by setting the RF received power level at −20 dBm. In [29] Silva *et al.* present an implantable WPT system to harvest RF energy for body-implantable devices. This system can also work with other communication systems. Another far field WPT example for feeding power to moving objects is conceived in [30] where the authors suggest a high-power RF transmitter at the $f = 16$ GHz range to wirelessly power a 92x92x29mm^3 drone using a frequency-scanned leaky-wave antenna on the drone. To the best of our knowledge, no conception of a far field SWIPT system, suitable for automation and transportation, has been reported in the literature apart from that in [29].

All the far-field WPT applications share the same flaw regarding the maximum allowable electromagnetic field power levels. For far-field propagation, the relation between the electric and magnetic field amplitudes becomes linear [12]. For the maximum allowable RF absorption levels for human tissues defined in the literature [31], it would not be possible, with simple treatment, to reduce the amplitude of one field without reducing the amplitude of the other.

For any propagation problem, to be considered as far field for automation and transportation applications, a basic distance of about 0.25 m could be assumed to calculate the corresponding frequency. In this case $\lambda = 0.25/10 = 2.5$ cm, and so the corresponding frequency shall be $f \approx 12$ GHz. For this frequency, the closest Industrial Scientific, and Medical (ISM) available bands are 5.8 GHz and 24.0125 GHz [32]. The power efficiency of solid-state devices, particularly for the higher band, is suboptimal and so the efficiency of a far-field WPT system for automation applications is, yet, compromised.

On the other hand, near-field WPT features high efficiency figures and has more degrees of freedom which helps to control the values of EM fields, generally the $\boldsymbol{E}$ field, without having the $\boldsymbol{H}$ field strictly defined as in the far field scenario.

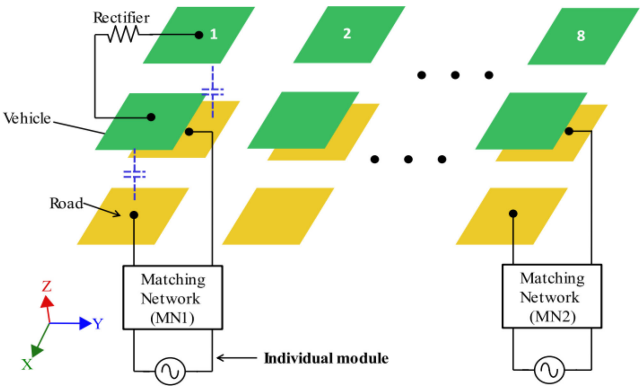

FIGURE 2. Schematic representation of capacitive WPT system made of repetitive Tx modules (yellow trapezoids) and the RX plates (green trapezoids) [33].

In this approach, however, the transmitted power between Tx and Rx is determined by the coupling factor between the two.

B. CAPACITIVE WPT

In this regime, the power is transferred from Tx to Rx using the $\boldsymbol{E}$ field. The transmission -or reception- system can be repeated as reported in [32] and shown in Fig. 2 to ensure continuous power supply for a moving vehicle. The Tx matching networks shown in Fig. 2 can be modified to make the system meet the $\boldsymbol{E}$ field safety requirements. When 180° alternating phase difference between adjacent elements is guaranteed, the fringing of the $\boldsymbol{E}$ field at the edges of the Tx and Rx system is reduced by 83% [33], thus both meeting the safety requirements and the needed transferred power levels. This study also shows an inverse relationship between the $\boldsymbol{E}$ field amplitude, and the operational frequency.

The modular design may be approached differently with the objective to maximize the transferred power from the Tx to Rx. In [34] Minnaert *et al.* propose a system that places less requirement on the Tx side making the received power maximization on the Rx side as shown in Fig. 3. A mathematical framework is assumed using N receivers and 1 transmitter as shown in Fig. 3(b). From the treatment of the presented mathematical model, which assumes zero coupling between the receiver modules, the admittance $Y_n = G_n + jB_n$may be given as:

$$Y_n = G_n + jB_n = g_{nn}\theta_N^2 + j \times 0 \tag{1}$$

where

$$\theta_N^2 = 1 + \frac{1}{g_{00}} \sum_{1}^{N} \frac{b_{0k}^2}{g_{kk}} \; : \; b_{0n} = \omega_0 C_{0n} \tag{2}$$

In this way, the received power can be optimized by changing the receiver loads Y_n to the values identified by (1), and (2).

As an example of SWIPT involving capacitive WPT, [35] offers a solution exploiting existing mobile phone antennas for simultaneous standard far-field communication and near-field capacitive WPT, when two mobile devices face each other.

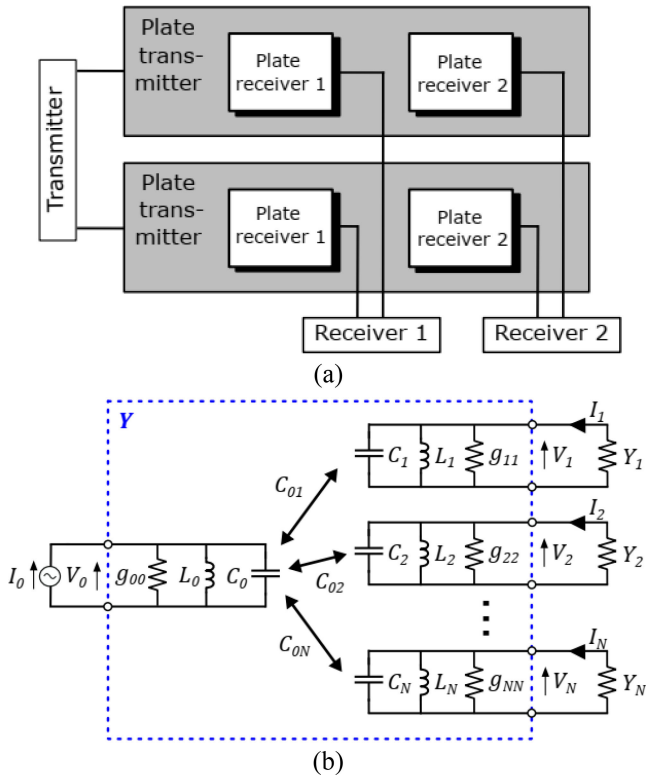

FIGURE 3. Schematic (a) and circuital (b) representation of an adaptive load WPT system made of repetitive Rx modules (aboard the moving object) and the TX plates (with constant loading conditions) [34].

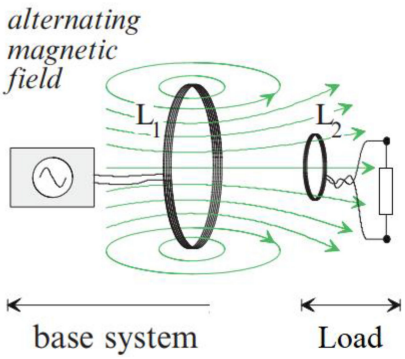

FIGURE 4. Schematic representation of WPT inductive coupling (Developed from [37] Courtesy of: Springer).

Because of the parasitic exploitation of the capacitive link, a medium-low efficiency is achieved.

C. INDUCTIVE WPT

The inductive coupling is the most widespread scheme for WPT and is based -in its simplest form as shown in Fig. 4- on coupling between two coils by the $\boldsymbol{H}$ field. To quantify the impact of the coils geometry on the electrical coupling between coil 1 and coil 2, the coupling factor k_{12} is used. It depends on the ratio between the mutual magnetic flux ϕ_{12} and the total magnetic flux ϕ_1. From mathematical equations [36], the coupling factor between the two coils, involving the mutual inductance M_{12} and the coils inductances may be found from:

$$k_{12} = \frac{M_{12}}{\sqrt{L_1 L_2}} = \frac{M_{21}}{\sqrt{L_1 L_2}} = k_{21} \tag{3}$$

As transportation systems require extended wireless power feed independently from the distance and the position between Tx and Rx, it has been necessary to put forward systems that ensure distance- and/or position-independent wireless power feed. This suggests the use of two -or more- consecutive Tx coils to feed a sliding Rx coil, which necessitates the study of coupling between more than two coils as will be seen in the following section. Inductive coupling remains the most promising and adopted mechanism for power transfer in SWIPT solutions in automation and transportation applications. For this reason, the aim of the paper is to focus on proposed solutions of this kind.

III. SLIDING WPT SYSTEM WITH LOAD- AND POSITION-INDEPENDENCY

As a first example of WPT solutions for both automation and transportation, the activity carried out in [38] is a significant step forward with respect to the state-of-the-art. The Inductive Power System (IPT) here presented is adjusted to deliver a constant output power of 100 W, thus addressing reliable and maintenance-free WPT systems for powering mass movers in industrial automation plants. Anyway, a scaled version for higher power budgets could be suitable for electrical vehicle energization on the move. Indeed, the system is able to provide an almost constant power to the receiver (Rx) while it is sliding over a sequence of aligned and static transmitters (Txs), therefore under significant variation of the loading condition offered by the Rx itself.

The novelties of this solution are manifold: i) it offers better performance in terms of invariance of the coupling among the coils while sliding than solutions with longer Tx [39]; ii) it proposes the "virtual" series connection between close Tx instead of a parallel connection as in [40], because of the optimal performance of this solution; iii) it needs for a DC feeding line and control logic along the powering path rather than a long RF feed distribution as in [41], thus reducing RF losses.

The co-design of the entire moving WPT system relies on three subsequent design phases: i) the electromagnetic design of the RF-to-RF link involving the planar coils layout; ii) the design of the class EF inverter acting as power source for the EM-based description of the wireless link of phase i); iii) the entire dc-to-dc design involving the two previous outputs for the final rectifying section design.

As regards the strategic step of the RF-to-RF link design, a fundamental role is played by the topologies of the involved coils: because of the movement of the Rx, Fig. 5 shows the reciprocal position between the Rx and a generic pair of Tx. In fact, the idea is to have just the couple of Txs facing the Rx active at a time.

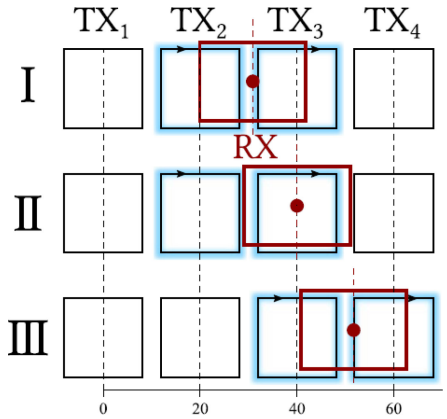

FIGURE 5. Schematic representation of reciprocal positions between the couple of series-connected TX coils (blue boxes) and the RX coil (red box) [38].

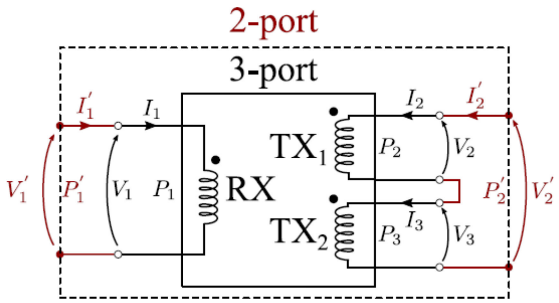

FIGURE 6. Circuital equivalent representation of the wireless link: the three-port network (black line) corresponds to the case of two independent TX coils; the two-port network (red line) corresponds to the adopted case of series-connected TX coils [38].

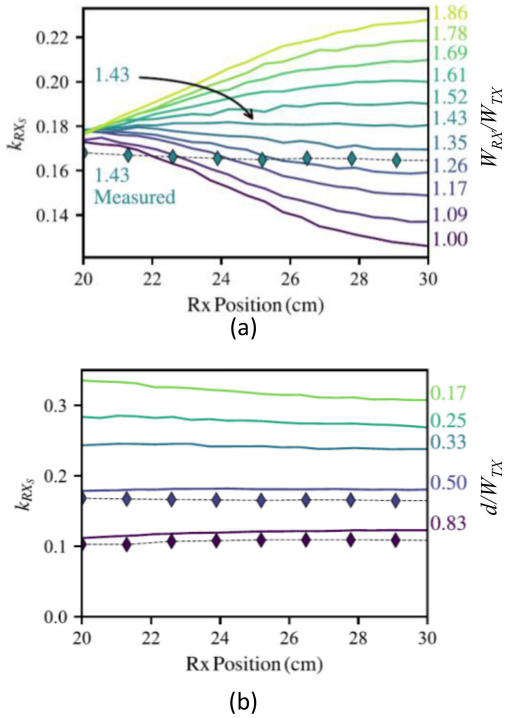

FIGURE 7. Coupling coefficient of the two-port link when the two TX coils are virtually connected in series: for different normalized (a) RX coil shape; (b) link distances. 20 cm and 30 cm correspond to the Rx axis aligned with the first TX axis and to Rx axis located in the middle between two TXs [38].

Starting from situation I, where the axis of the Rx is in between the two Tx, and reaching the situation II, where the axis of the Rx is aligned with the center of the second Tx, the system geometry is indefinitely repeated identically.

First, the advantage of a series connection of the Tx pair instead of their parallel is demonstrated in [42]. Then, the resulting two-port network shown in Fig. 6 is analyzed to achieve the resulting coupling factor expression:

$$k_{RX\_series} = \frac{1}{\sqrt{2}} \frac{k_{RX1} + k_{RX2}}{\sqrt{1 + k_{TX}}} \tag{4}$$

Where, according to (3), k_{TX} is the coupling factor between the two TX coils and k_{RX1} and k_{RX2} are the coupling factor between the RX and the TX_1 and TX_2 coils, respectively [38].

As a final step of this phase, an extensive full-wave simulation campaign is carried out by changing the Rx position and dimension, and fixing the Tx dimension in order to operate at 6.78 MHz. The plots of (4) for different positions and Rx dimension are reported in Fig. 7(a), (b): Fig. 7(a) reports the coupling factor with the Rx shape as a parameter, thus providing the optimum constant behavior for W_{RX}/W_{TX} =1.43, corresponding to W_{RX} =17.2 cm being the fixed W_{TX} = 12 cm; whereas Fig. 7(b) provides the coupling factor for the optimal shape as a function of the Rx distance from the Tx (d): this figure demonstrates that the flatness of the inductive coupling is maintained by varying the link distance.

It is worth noticing that the presented EM design is referred to the horizontal misalignment under exam with series connection of the Tx. A variation from this situation (rotation or vertical displacement between Rx and Tx) would produce a different optimal shape.

As regards the RF source on the Tx side, a Class EF inverter deploying a GaN HEMT (similar to [14]) is used. In order to minimize the losses, the zero-voltage-switching (ZVS) condition is mandatory: the optimization of the nonlinear source (one for each Tx) is then carried out focusing on the simultaneous achievement of the ZVS condition and of the constant output current for variable loads. The latter condition is the one allowing the "virtual" series connection between the two active Txs, while the Rx is sliding over them, thus while the load is significantly changing.

With respect to a standalone Tx (as in [14]) in this case the coupling between the two neighboring active Txs must be taken into account, because the effective inductances, loading them, are different from those at the output of a stand-alone inverter.

Moreover, in the present application the unwanted currents induced in the non-active Tx must be minimized, too, to reduce the active inverter losses and detuning. For this reason the final layout of the class EF inverter is the one reported in

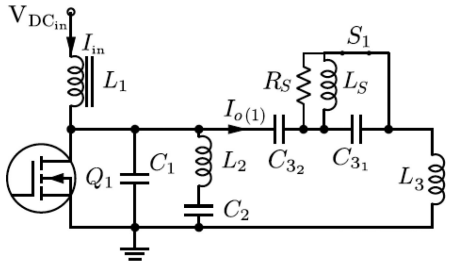

FIGURE 8. Scheme of the class EF inverter. The additional switch S1 is closed (inverter OFF and detuned) [38].

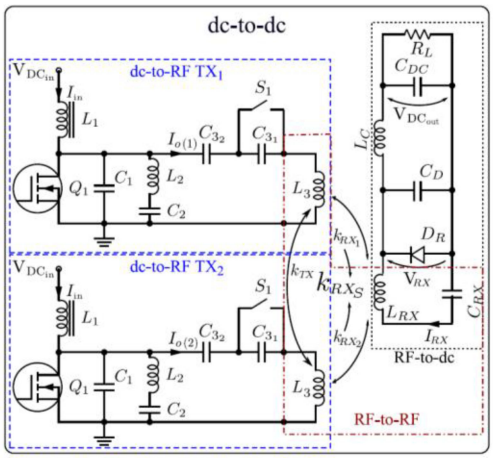

FIGURE 9. Entire system representation, from dc to dc. L_3 are the TX coils, coupled with the RX coil (L_{RX}) which is connected to a class E rectifier closed on a variable load (R_L) [38].

Fig. 8, where S_1 represents a switch, and the series capacitance C_3 has been split in two contributions C_{32} and C_{31} (with $C_{32} > C_{31}$): in this way, if the inverter is OFF (S_1 closed) it is strongly detuned and its current is minimized.

Finally, the rectifier on the Rx side has to provide a constant dc output voltage and a purely resistive impedance in the expected power and load ranges. This challenging task cannot be reached with a standard class E rectifier [43], because of the varying reactance while changing the Rx position. For this reason, a Harmonic Balance (HB) analysis of the whole system (from dc to dc) shown in Fig. 9 is carried out, for different Rx loads.

As per the nonlinear devices of Fig. 9, the FET Q1 is the GaN System GS66504B Enhancement HEMT and the diode DR is the Schottky SiC Wolfspeed/CREE C3D1P7060Q.

The final setup is shown in Fig. 10, where a detail of the single Tx module as well as of the whole system (with 4 Tx) is given.

As representative results of the WPT system at 6.78 MHz for on-the-move powering, Figs. 11 and 12 report the rectified output voltage for 70 V of DC input, for different positions of the Rx, and the overall dc-to-dc efficiency as a function of the dc output power, respectively.

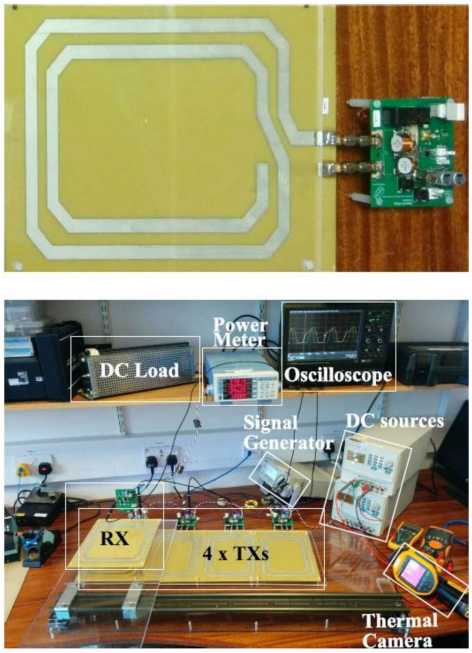

FIGURE 10. Photo of the TX module (upper side). Photo of the whole system for dc-to-dc measurements (lower side) [38].

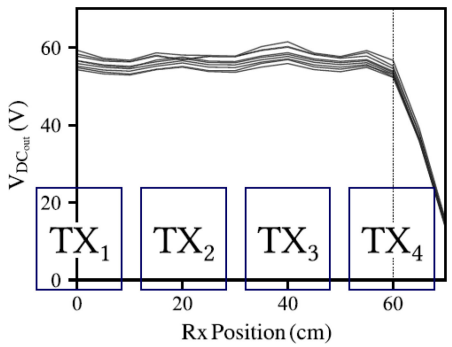

FIGURE 11. Output dc voltage as a function of the RX coil position, with the resistive load (R_L) as an additional varying parameter [38].

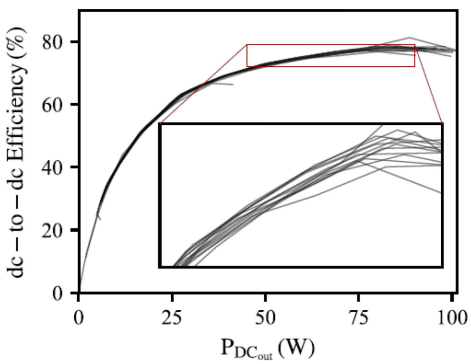

FIGURE 12. dc-to-dc system efficiency as a function of the output dc power varied by sweeping the R_L value from 30 to 500 Ω. Each curve corresponds to a different RX coil position [38].

Fig. 11 clearly states that the constant dc output voltage is guaranteed only if the virtual series between the Tx is assured: as soon as it is not (after the 4th Tx) the performance drastically worsens. The different curves of Fig. 12 are due to different Rx positions: in this case, the load resistance is varied from 30 to 500 ohm, thus mimicking the output power sweep. An efficiency of 80% is achieved for the targeted output power of 100 W.

IV. MOVING SWIPT IN A RAILWAY SYSTEM

Another interesting application where SWIPT is applied to transportation is the one directly derived from the European railway safety system, called Balise Transmission Module (BTM). In this system, a WPT link is established between two coils resonating at $f_{WPT} = 27.095$ MHz: the active one (BTM) is on the train and energizes the passive one (the Eurobalise) placed on the track when the two are facing each other. The same wireless link is also exploited, in the opposite direction from the Eurobalise to the BTM, for communication purposes through two co-located new coils, resonating at $f_{COM} = 4.234$ MHz.

As the previous example, this case involves a varying WPT link, too: in fact, the movement of the train makes the inductive coupling between the coils a variable one. Moreover, an additional issue raises the level of difficulty of the present design: the commercially available balises on the track are different and the distance between the transmitting power coil and the receiving one can vary, depending on the installation, from a minimum distance of about 20 cm to a maximum one of 40 cm.

This problem has received attention from the specialized literature: in [22] an analytical model of the electromagnetic coupling between the loops is proposed and verified through finite-element analysis; an additional channel for the communication link is proposed in [24] for an increased data capacity, but the analysis is still related to the coils, only. Full-wave analysis of the electromagnetic susceptibility related to the sole communication link is managed in [44]. The framework in [45] offers an analysis of the unwanted interferences between the balise on the track and other existing train positioning systems (i.e., Euroloop). Many solutions from the algorithmic point of view are also offered for the uplink (or communication link) of the BTM and the idea of the "virtual" balise is presented in [46] deploying onboard sensors and the Global Navigation Satellite System.

However, a complete design of the overall link, also considering the SWIPT scenario is still missing, and a first attempt is provided in [47]. In the following, the design choices and their numerical implementation for a realistic application are briefly summarized.

The first choice relates to the power amplifier to be connected to the power coil. A class E inverter is the adopted one, mainly for its demonstrated independency on the load [15], representing a strategic need for the present application: both the unknown characteristics of the incoming balise and the link distance can be accounted for. The topology of the inverter is given in Fig. 13, where a π network has been added for matching reasons.

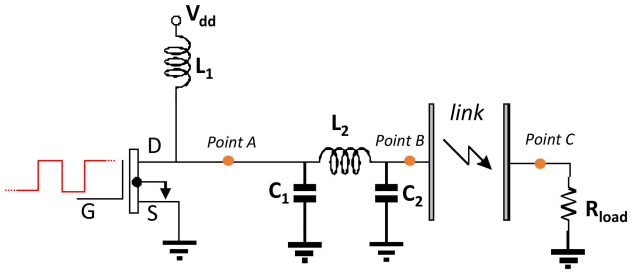

FIGURE 13. Class E inverter scheme, including the π matching network and the wireless link.

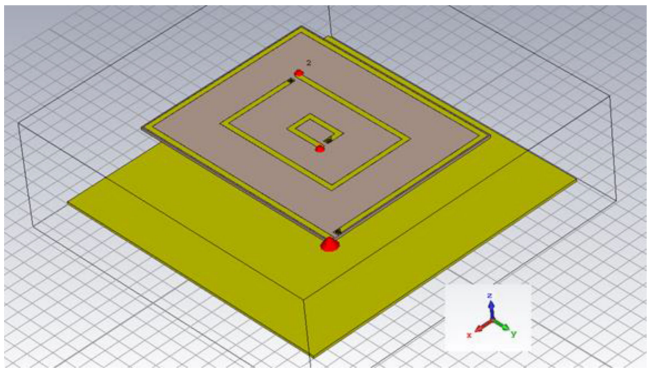

FIGURE 14. 3D view of the shielded multi-coil on-board sub-system.

The crucial role of the switching nonlinear device is played again by a GaN HEMT device: the GS66508b from GaN Systems. The drain of the device is connected to the DC bias source (V_{dd}), whereas the gate port is driven by a train of rectangular pulses (between 0 and 5 V) of period $T_{WPT} = 1/f_{WPT} \approx 370$ us). This device assures low losses, provided that the soft-switching conditions [48] are fulfilled: according to these conditions, at a given instant, the product of the current flowing through the switch and the voltage across it should be zero (or as low as possible), i.e., the power lost in the switch is very small. From a mathematical point of view, this means that, when the device current is different from 0 (i.e., the $V_{GS} = 5$ V) the ZVS and ZDS (zero derivative switching) must be simultaneously satisfied:

$$\begin{cases} V_{DS}(2\pi) = 0 \rightarrow ZVS \\ \frac{dV_{DS}(\omega t)}{d(\omega t)}|_{\omega t = 2\pi} = 0 \rightarrow ZDS \end{cases} \tag{5}$$

The second choice refers to the coils layout and placement: a planar topology with 70 μm-thick copper is selected. The power coil (port #1) and the communication one (port #2) are placed on the same substrate (common FR-4) as depicted in Fig. 14: they have quite different dimensions (power coil: 300 mm x 240 mm; communication coil: 180 mm x 120 mm) in order to minimize the unwanted electromagnetic coupling between the two ports to preserve the SWIPT operation. In Fig. 11 an additional smaller coil (54 mm x 36 mm) is placed

in the center of the substrate: this is the test coil, operating at a further different frequency (about 6 MHz) introduced to continuously check the effectiveness of the power link, for safety reasons. Using 35 μm copper plating, a line width of 7 mm leads to the lowest parasitic resistance of the power coil ($R_p = 36$ mΩ). Moreover, an inductance of about 1 μH, as suggested in [49] is obtained with a single turn coil (Fig. 14): a two-turn layout, despite the smaller footprint, would have a higher parasitic resistance and a closer self-resonance to be taken under control. All the coils are made resonant with the corresponding proper lumped series capacitance. The inductance (derived from full-wave simulation) and lumped capacitance values, for the power and the communication coils are: 896 nH, 38.5 pF, 398 nH, 3.5 nF, respectively.

The back plane, whose area is wider than the power-coil one, is an aluminum shield placed 80 mm far from the FR-4 substrate, foreseen for immunity reason of the BTM from the strong electromagnetic fields generated by the train engine.

As a further precaution, trapping filters providing a series resonance at the unwanted frequency are also placed at the communication (#2) and test (#3) ports.

The full-wave description of the wireless link is then considered as the realistic load of the inverter: as a receiving coil, a generic planar loop, as the one adopted to test the commercial balises [50] is considered. The receiving balise power port is closed on a 50 Ω resistor, mimicking the input port of a generic receiver. The link is electromagnetically characterized for different distances (in the range 20–40 cm) and different longitudinal misalignments.

Because of the highly nonlinear behavior of the switching amplifier, a wideband electromagnetic-characterization of the link is needed (from 0 to 550 MHz, thus including up to the 20th harmonic of the fundamental): this fact has been experimentally proved to have a big impact on the overall system performance during the design procedure.

It is worth mentioning that a preliminary optimization of the system was not satisfactory, because of the too high electromagnetic coupling between the power coil and the other two smaller and nested coils, despite of the adopted 180°-rotation of the neighboring coils to increase the ports distance (see. Fig. 14). Instead of resorting to a re-design of the coils and the exploitation of a bulky structure with different layers for the different coils, a simpler circuital solution is followed by connecting trapping filters at the input coil ports. In particular, for the reduction of the high coupling at 27 MHz due to the strong signal transmitted by the power coil, a parallel branch (resonant at 27 MHz) is series connected to the communication and test coil ports: the high impedance offered by the parallel resonator prevents the power signal from reaching the undesired coils. The effectiveness of this solution is demonstrated at the end of this section.

Once the system blocks have been established, an HB optimization of the lumped components of the inverter, reported in Fig. 13, is carried out, asking for the simultaneous satisfaction of the following goals: i) maximum power level at 27 MHz at the input port of the wireless link equal to 30W; ii) the ZVS and ZDS condition for low losses in the switch; iii) maximum inverter efficiency (given by the ratio of the AC power delivered to the power coil and the dc power needed at the input port), when it has to send the power (i.e., when the balise is perfectly aligned with the power coil or the misalignment is in the range ± 10 cm); iv) minimization of the AC transmitted power in the absence of the coupled balise. The advantage of optimizing the system by means of the HB technique instead of traditional time-domain simulation relies in the simultaneous control of the large nonlinear dynamic of the switch and the strongly frequency dependent behavior of the link [40].

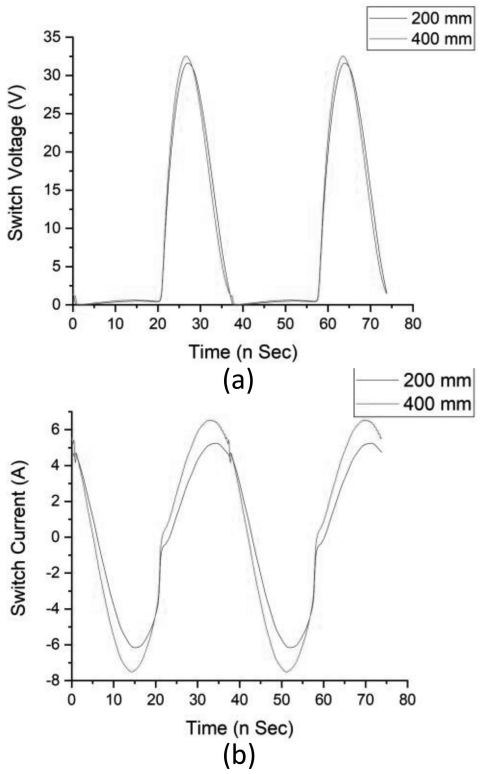

FIGURE 15. Voltage and current waveforms at the drain terminal of the GaN transistor for two link distances.

The final optimum parameters of the inverter of Fig. 13, driven by a 50%-duty-cycle-27MHz pulse at the gate terminal of the GaN HEMT, are: $L_1 = 80$ μH, $L_2 = 23.5$ nH, $C_1 = 228$ pF, and $C_2 = 5$pF, $V_{dd} = 9$ V.

As a demonstration of the proper performance of the system when varying the link distance, Fig. 15(a), (b) shows the waveforms of the voltage and current just after the switch (point A in Fig. 13):

The almost identical shape of these waveforms for the two link distances under test (20 and 40 cm) demonstrates the load-independent behavior of the system. One can note that the ZVS condition is not rigorously verified, hence some losses occur: in fact, the current is not zero when the voltage is different from zero. This is due to the realistic description of the GaN device through its nonlinear model, as testified

by the same simulation with an ideal switch model: in ideal conditions the inverter efficiency and the DC input power) is more than 90%, whereas it decreases up to 75% with the real switch.

As a final test, the optimized inverter is connected to the same link, but without the trapping filters. As expected, the performance drastically drop: if we consider the 200 mm distance case, the power coupled to the communication and test coils is 19 W and 70 mW without the trapping filters, and 0.7 W and 2 mW with their inclusion.

V. SIMULTANEOUS INDUCTIVE ENERGY AND CAPACITIVE INFORMATION TRANSFERS IN AUTOMATIC INDUSTRIAL MACHINERY

As a further example of SWIPT for industrial scenarios, in [41] a smart exploitation of a self-resonant capacitive near-field link at UHF for data transfer is presented, while adopting a co-located standard coupled coils for the wireless transmission of the power. The capability to make use of the same wireless link for both the transmissions (data and power) relies on the high decoupling between the two adopted mechanisms: capacitive power transfer (CPT) (i.e., through electric field) at UHF, which is complementary to the inductive power transfer (IPT) (e.g., through magnetic field) at LF (50 kHz).

The usage of UHF for the near-field capacitive link is not a hazardous choice because in many contactless industrial applications the distance involved between the energy source and the electric load is reduced (a few millimeters). In the present application, the load is a passive resistor temperature sensor and split-ring resonators (SRRs) are adopted at each side of the wireless chain, free to rotate with respect to each other, for the readout of the remote temperature sensor.

In Fig. 16(a) the perspective view of the co-located power and data links is given: the ferrite cavity is filled with metallic windings for the standard inductive coupling made resonant at 50 kHz and able to transfer power in the kW range; in order to simultaneously and remotely sensing the operating conditions of the far end of rotary tools capacitive SRR with their ground plates are included in the winding area of rotating cores. Detailed view of the SRR layout is provided in Fig. 16(b).

The exploitation of 868 MHz as data frequency, makes the corresponding link not a rigorously capacitive link: at this frequency, the plates of the SRR behave as strip conductors whose length is comparable with the wavelength. Therefore, they also exhibit a self- and mutual-inductive behavior. However, the use of SRR in near-field wireless links for data (and power) transfer has been already demonstrated [42]. In this case, they are also part of the remote sensing apparatus: differently from [43], where the SRRs are used as passive sensing elements, here they allow the feedback loop for data communication.

Fig. 17 shows the near-field link realized with two faced SRRs with their own ground plate. d represents the link distance (=0.6 mm for the present application), whereas α is the relative angular position of the outer strip slots position. An electromagnetic optimization of the facing SRRs geometries

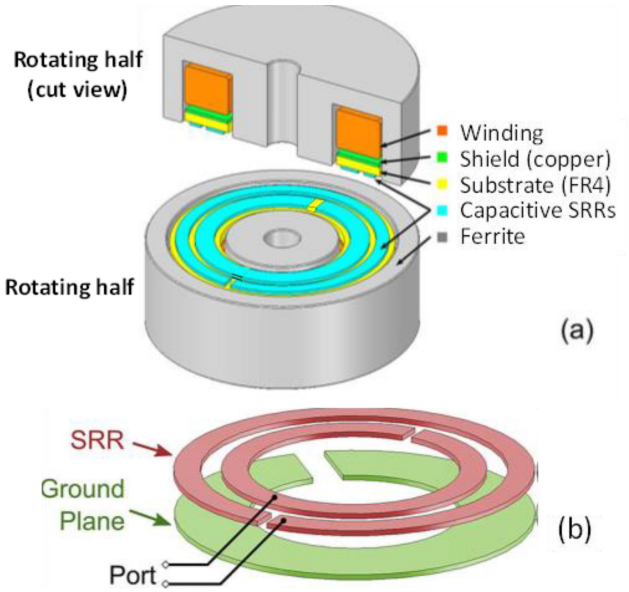

FIGURE 16. View of the wireless power and information transfer device: (a) cut view of the complete sub-system; (b) detail of the grounded SRR adopted for information transfer [51].

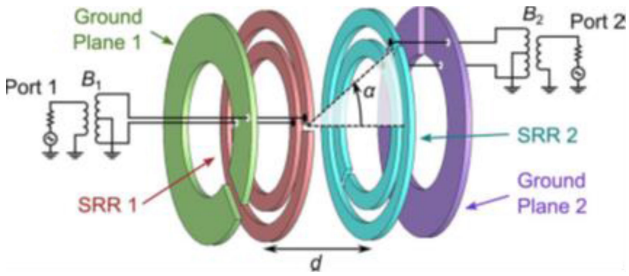

FIGURE 17. Communication link between the two faced SRRs [51].

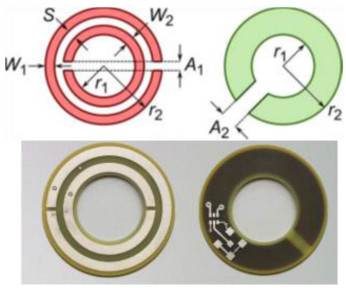

Symbol	Value	Symbol	Value
S	2 mm	A_1	1 mm
W_1	2.5 mm	A_2	3 mm
W_2	2.5 mm	t	1.12 mm
r_1	10 mm	d	0.6 mm
r_2	17 mm	a	45 °

FIGURE 18. Geometric details and photo of the realized SRR [51].

is also carried out in order to make the link resonant at 868 MHz: note that the angular parameter α can be effectively used to tune the resonance frequency of the link. The final layout of the SRRs together with their dimension is given in Fig. 18, where a picture of the first prototype, realized on FR4 Panasonic four-layer R1566/R1551 substrate (ε_r= 5.0, tan δ = 0.015), is also shown.

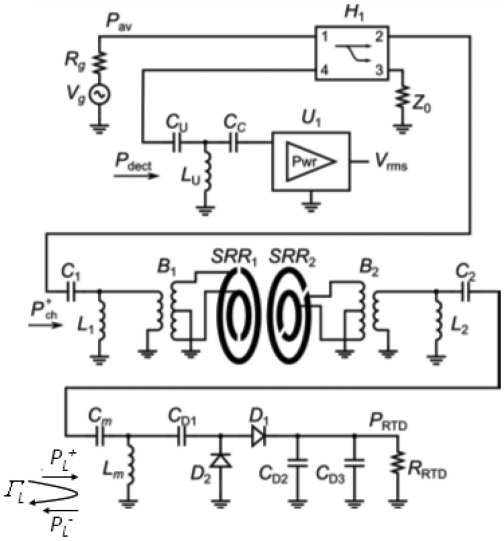

FIGURE 19. Circuit-equivalent description of the UHF wireless link for passive temperature sensing [51].

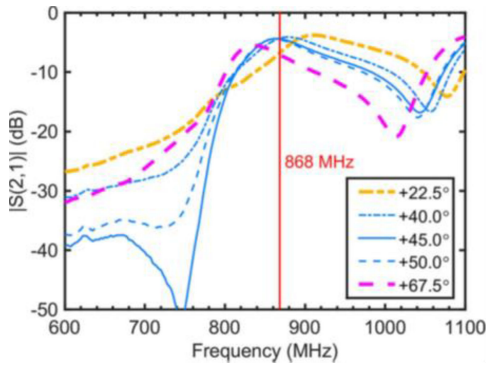

FIGURE 20. Measured transmission coefficient of the system in Fig. 17 while rotating [51].

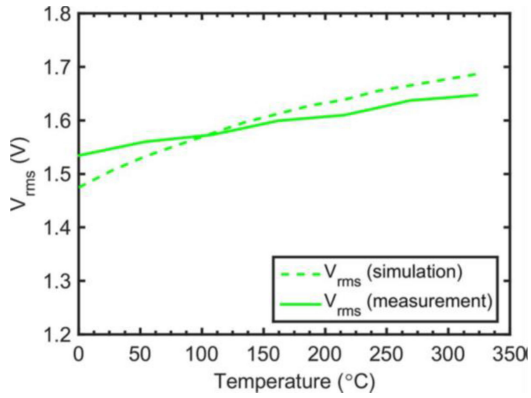

FIGURE 21. Comparison of the measured and predicted relationships between the power detector output voltage and the corresponding sensed temperature [51].

The SRRs are used as chipless RFID tags: it is well known that the field backscattered by this kind of tag (in particular, changes in the phase content) can be unpredictably affected by the environment if standard links, several wavelength-long, are involved [44]. However, in the present case, the channel is short, invariant, and well-known: hence, its model can be included in the system and, consequently, the uncertainties can be removed. For these reasons, the exploitation of a resistive temperature sensor (RTD) as a variable load of the link, allows to make use of the variation of the reflection coefficient Γ_L at the transmitter side as an indication of the temperature variation. In order to emphasize the effect of Γ_L variations, the receiving part must be designed in such a way to operate in maximum sensitivity mismatching (MSM) conditions, far from the usual conjugate matching conditions.

The overall system is schematically represented in Fig. 19. From figure's inspection, it is possible to note the presence of a rectifying section of a passive RFID tag at the receiver side: this is an original solution adopted to smooth the severe parasitic effects of the RTD sensor, which is an uncommon load for RF applications. On the transmitter side there is also a directional coupler with a low coupling factor *C*, which exploits the isolated port (# 4 in Fig. 19) to decouple the reflected power entering port # 2 from the other power contributions, according to the rule:

$$C = \log_{10}\left(\frac{P_2}{P_4}\right) = -20\log_{10}|S_{24}| \qquad (6)$$

The previous formula justifies the need for a low C, since a high $|S_{24}|$ is mandatory for the detection of the reflected power variations.

A nonlinear optimization of the entire system is then carried out, by resorting to the Quasi-Newton optimization algorithm in the framework of the HB technique [45]: during this phase, the available input power and the parameters of the MSM network (P_{av}, and C_m, L_m, respectively, in Fig. 16) are used as design variables. The whole set of parameters is also given in Fig. 18. A quite high P_{av} value is obtained (=10 dBm): however, this is not a big concern for the present application, where the main goal is to get rid of sensor reading circuitry and power supply in the high temperature sensor region, rather than to minimize power consumption.

As a preliminary experiment, the wireless link is tested: first, the measured scattering parameters of the link of Fig. 17 are compared with the corresponding full-wave results and an excellent agreement is reached [41]. Then the link is characterized while varying the angle α. Fig. 20 indicates that, within an angle interval of 10° around the 45° reference, the same link performance (in terms of transmission coefficient) are guaranteed, thus ensuring a safe accuracy of temperature measurement during the receiver rotation.

As regards the whole system, the intended performance is to detect temperature variations in the range [0÷323] °C, corresponding to an RTD variation in the range [1÷2.2] kW. As a first comment, the $P_{av} = 10$ dBm allows to have around [−2.5,−0.5] dBm at the rectifier input port depending on the load value: this power range corresponds to the lowest

reduction in the load reflection coefficient dynamics due to the nonlinear network, and justifies the adopted P_{av} value. The corresponding power variation at the detector input port (the AD8361 manufactured by Analog Devices) spans between −6.22 and −5.60 dBm, resulting in a dc voltage varying between 1.53 and 1.65 V. Fig. 21 shows these measurements, superimposed to the simulated results, as a function of the load temperature: the slight nonlinear, but expected, behavior is due to the rectifier. The resulting average sensitivity is 0.35 mV/°C, having a detected voltage range of 113 mV for temperature variations between 0 °C and 323 °C.

VI. CONCLUSION

In this work some recent WPT systems, exploiting near-field electromagnetic coupling, have been reviewed. They were developed for specific applications in the industrial and transportation sectors. In such complex environments there are many system variables, such as the TX and RX respective location and the loading conditions, that need be considered randomly variable without affecting significantly the WPT operations. To reach this goal a suitable design approach has been described, able to combine the wireless channel rigorous description with the nonlinear behaviour of its terminations, the transmitting and receiving sub-systems. Suitable circuital topologies for the transmitters and the receivers have been proposed to be robust with respect to loading conditions variations. Their combinations with the EM-based description of the wireless link has been adopted to carry out the optimization of the entire system. Differently from more traditional approaches the operating frequency in the low MHz range has been chosen demonstrating the twofold advantage of wireless link miniaturization and high energy transfer rate.

REFERENCES

[1] D. Mcginnis, "What is the fourth industrial revolution?" 2018. Accessed: Sep. 11, 2020. [Online]. Available: https://www.salesforce.com/blog/2018/12/what-is-the-fourth-industrial-revolution-4IR.html

[2] M. Executive, "Transport uses 25 percent of world energy," 2015. Accessed: Sep. 11, 2020. [Online]. Available: https://www.maritime-executive.com/article/transport-uses-25-percent-of-world-energy

[3] A. Szajna and R. Kielec, "The new way of maintenance and service of the production lines with the application of augmented reality and artificial intelligence," in *Proc. Vis. 2020 Sustain. Econ. Develop. Appl. Innov. Manage.*, 2018, pp. 5877–5885.

[4] A. Bhardwaj *et al.*, "Who's the boss? Arbitrating control authority between a human driver and automation system," *Transp. Res. F, Traffic Psychol. Behav.*, vol. 68, pp. 144–160, Jan. 2020.

[5] Alstom, "World-first: Automatic train operation for regional passenger trains to be tested in Germany," 2020. Accessed: Sep. 14, 2020. [Online]. Available: https://www.alstom.com/press-releases-news/2020/5/world-first-automatic-train-operation-regional-passenger-trains-be

[6] M. A. Hossain, R. Md Noor, K. A. Yau, I. Ahmedy, and S. S. Anjum, "A survey on simultaneous wireless information and power transfer with cooperative relay and future challenges," *IEEE Access*, vol. 7, pp. 19166–19198, 2019.

[7] F. Jameel *et al.*, "A technical review of simultaneous wireless information and power transfer (SWIPT)," in *Proc. Int. Symp. Recent Adv. Elect. Eng.*, Islamabad, 2017, pp. 1–6.

[8] B. Clerckx, A. Costanzo, A. Georgiadis, and N. Borges Carvalho, "Toward 1G mobile power networks: RF, signal, and system designs to make smart objects autonomous," *IEEE Microw. Mag.*, vol. 19, no. 6, pp. 69–82, Sep./Oct. 2018.

[9] N. Tesla, *Apparatus for Transmitting Electrical Energy*, US1119732A Patent, 1907.

[10] A. D. Stokes and D. K. Sweeting, "Electric arcing burn hazards," *IEEE Trans. Ind. Appl.*, vol. 42, no. 1, pp. 134–141, Jan./Feb. 2006.

[11] A. Kurs *et al.*, "Wireless power transfer via strongly coupled magnetic resonances," *Science*, vol. 317, no. 5834, pp. 83–86, Jul. 2007.

[12] D. Masotti, M. Shanawani, and A. Constanzo, "Smart beamforming techniques for 'On demand' WPT," in *Wireless Power Transmission for Sustainable Electronics*, N. Borges Carvalho, A. Georgiadis, Eds. New York, NY, USA: Wiley, 2020, pp. 57–84.

[13] D. C. Yates *et al.*, "Design of 3 MHz DC/AC inverter with resonant gate drive for a 3.3 kW EV WPT system," in *Proc. IEEE 2nd Annu. Southern Power Electron. Conf.*, Auckland, 2016, pp. 1–4.

[14] S. Aldhaher *et al.*, "Load-independent class EF inverters for inductive wireless power transfer," in *Proc. IEEE Wireless Power Transfer Conf.*, 2016.

[15] S. Aldhaher, D. C. Yates, and P. D. Mitcheson, "Load-independent class E/EF inverters and rectifiers for MHz-switching applications," *IEEE Trans. Power Electron.*, vol. 33, no. 10, pp. 8270–8287, Oct. 2018.

[16] O. Abdelatty *et al.*, "Exploiting nonlinearity to design robust wireless power transfer and wideband RF energy harvesting," in *Proc. IEEE Wireless Power Transfer Conf.*, Montreal, QC, Canada, 2018, pp. 1–4.

[17] D. H. Kim and D. Ahn, "Optimization of capacitive wireless power transfer system for maximum efficiency," *J. Elect. Eng. Technol.*, vol. 15, no. 1, pp. 343–352, Jan. 2020.

[18] G. A. Covic and J. T. Boys, "Inductive power transfer," *Proc. IEEE*, vol. 101, no. 6, pp. 1276–1289, Jun. 2013.

[19] B. Luo, T. Long, L. Guo, R. Dai, R. Mai, and Z. He, "Analysis and design of inductive and capacitive hybrid wireless power transfer system for railway application," *IEEE Trans. Ind. Appl.*, vol. 56, no. 3, pp. 3034–3042, May/Jun. 2020.

[20] Y. S. Chen and C. W. Chiu, "Maximum achievable power conversion efficiency obtained through an optimized rectenna structure for RF energy harvesting," *IEEE Trans. Antennas Propag.*, vol. 65, no. 5, pp. 2305–2317, May 2017.

[21] J. M. Arteaga, S. Aldhaher, G. Kkelis, C. Kwan, D. C. Yates, and P. D. Mitcheson, "Dynamic capabilities of multi-MHz inductive power transfer systems demonstrated with batteryless drones," *IEEE Trans. Power Electron.*, vol. 34, no. 6, pp. 5093–5104, Jun. 2019.

[22] T. Wang *et al.*, "Modeling and optimization for balise coupling process in high speed railway," in *Proc. 7th IEEE Int. Symp. Microw., Antenna, Propag. EMC Technol.*, pp. 176–179, 2017.

[23] S. B. Lee *et al.*, "Optimization of the wireless power transfer system in an electric railway," in *Proc. IEEE Wireless Power Transfer Conf.*, pp. 158–161, 2014.

[24] L. F. Zhu *et al.*, "Mutual coupling research of multi-antenna in dual-channel balise," in *Proc. IEEE Int. Conf. Intell. Transp. Syst.*, pp. 2200–2204, 2015.

[25] D. Liang *et al.*, "Research on dynamic pattern of balise Up-link signal based on the electromagnetic field theory," in *Proc. IEEE Int. Conf. Intell. Rail Transp.*, pp. 155–159, 2013.

[26] Y. L. Song *et al.*, "Fast prediction model for the susceptibility of balise transmission module system based on neural network," in *Proc. Int. Conf. Electromagn. Adv. Appl.*, pp. 445–448, 2019.

[27] J. Garnica, R. A. Chinga, and J. S. Lin, "Wireless power transmission: From far field to near field," *Proc. IEEE*, vol. 101, no. 6, pp. 1321–1331, Jun. 2013.

[28] J. Kim *et al.*, "Experimental analysis of harvested energy and throughput trade-off in a realistic SWIPT system," in *Proc. IEEE Wireless Power Transfer Conf.*, pp. 1–5, 2019.

[29] V. F. Silva *et al.*, "Shared wireless link co-design for implantable device with far-field wireless power transfer," in *Proc. IEEE Int. New Circuits Syst. Conf.*, 2019.

[30] J. L. Gómez-Tornero *et al.*, "Design of Ku-band wireless power transfer system to empower light drones," in *Proc. IEEE Wireless Power Transfer Conf.*, Aveiro, 2016, pp. 1–4.

[31] Environmental Health Directorate, "Limits of human exposure to radiofrequency electromagnetic energy in the frequency range from 3 kHz to 300 GHz," Safety Code, Canada, 1999.

[32] Federal Communications Commission, Table of Frequency Allocations Chart, *ARTICLE 5 Frequency Allocations Standard ITU Radio Frequencies, CHAPTER-II*, 2016. [Online]. Available: https://www.fcc.gov/engineering-technology/policy-and-rules-division/general/radio-spectrum-allocation

[33] I. Ramos *et al.*, "Near-field capacitive wireless power transfer array with external field cancellation," in *Proc. IEEE Wireless Power Transfer Conf.*, Aveiro, 2016, pp. 1–4.
[34] B. Minnaert *et al.*, "Optimizing the power output for a capacitive wireless power transfer system with N receivers," in *Proc. IEEE Wireless Power Transfer Conf.*, pp. 351–354, 2019.
[35] M. Del Prete *et al.*, "Seamless exploitation of cell-phone antennas for near-field WPT by a frequency-diplexing approach," *IET Microw. Antennas Propag.*, vol. 11, no. 5, pp. 649–656, Apr. 2017.
[36] A. Pacini, "Design of novel systems for position independent energy and data transfer," Ph.D. dissertation, Alma Mater Studiorum, Università di Bologna, 2019.
[37] K. Van Schuylenbergh and R. Puers, *Inductive Powering: Basic Theory and Application to Biomedical System*. New York, NY, USA: Springer Science & Business Media, 2009.
[38] A. Pacini *et al.*, "Load- and position-independent moving MHz WPT system based on GAN-distributed current sources," *IEEE Trans. Microw. Theory Techn.*, vol. 65, no. 12, pp. 5367–5376, Dec. 2017.
[39] J. Shin *et al.*, "Design and implementation of shaped magnetic-resonance-based wireless power transfer system for roadway-powered moving electric vehicles," *IEEE Trans. Ind. Electron.*, vol. 61, no. 3, pp. 1179–1192, Mar. 2014.
[40] A. Pacini *et al.*, "Design of a position-independent end-to-end inductive WPT link for industrial dynamic systems," in *Proc. IEEE MTT-S Int. Microw. Symp.*, pp. 1049–1052, 2017.
[41] Z. Zhang and K. T. Chau, "Homogeneous wireless power transfer for move-and-charge," *IEEE Trans. Power Electron.*, vol. 30, no. 11, pp. 6213–6220, Nov. 2015.
[42] A. Pacini *et al.*, "Geometry optimization of sliding inductive links for position-independent wireless power transfer," in *Proc. IEEE MTT-S Int. Microw. Symp.*, 2016.
[43] M. K. Kazimierczuk, "Analysis of class E Zero-voltage-switching rectifier," *IEEE Trans. Circuits Syst.*, vol. 37, no. 6, pp. 747–755, Jun. 1990.
[44] Y. Wen *et al.*, "Study on the electromagnetic susceptibility of balise transmission module system," in *Proc. Int. Conf. Electromagn. Adv. Appl.*, pp. 667–670.
[45] R. Sharma *et al.*, "Crosstalk reduction in balise and infill loops in automatic train control," in *Proc. Int. Conf. Intell. Eng. Syst.*, Budapest, 2007, pp. 39–44.
[46] M. Lauer and D. Stein, "A train localization algorithm for train protection systems of the future," *IEEE Trans. Intell. Transp. Syst.*, vol. 16, no. 2, pp. 970–979, Apr. 2015.
[47] G. Murtaza *et al.*, "Optimization of a 27 MHz wireless power transmitter for an unknown receiver," in *Proc. URSI GASS*, Rome, Italy, pp. 1–4.
[48] M. K. Kazimierczuk and D. Czarkowski, *Resonant Power Converters*. New York, NY, USA: Wiley, 2012.
[49] C. Florian *et al.*, "Theoretical and numerical design of a wireless power transmission link with GAN-based transmitter and adaptive receiver," *IEEE Trans. Microw. Theory Techn.*, vol. 62, no. 4, pp. 931–946, Apr. 2014.
[50] *ERTMS/ETCS Test Specification for Eurobalise FFFIS*, EUAF, Railways Standard Set of Specifications 3, ETCS B3 R2 GSM-R B1, Subset-085v3.0.0, 2012.
[51] R. Trevisan and A. Costanzo, "A UHF near-field link for passive sensing in industrial wireless power transfer systems," *IEEE Trans. Microw. Theory Techn.*, vol. 64, no. 5, pp. 1634–1643, May 2016.